Ligand, Cofactor, and Residue Vibrations in the Catalytic Site of Endothelial Nitric Oxide Synthase†

W. John Ingledew,*,‡ Susan M. E. Smith,§ Y. T. Gao,§ R. J. Jones,§ John C. Salerno,§ and Peter R. Rich||

School of Biology, University of St. Andrews, St. Andrews KY16 9JF, U.K., Biology Department, Rensselaer Polytechnic Institute, Troy, New York 12180, and Glynn Laboratory of Bioenergetics, Department of Biology, University College London, Gower Street, London WC1E 6BT, U.K.

Received September 29, 2004; Revised Manuscript Received January 6, 2005

ABSTRACT: A study of bovine endothelial nitric oxide synthase by Fourier transform infrared (FTIR) spectroscopy in the 1000−2500 cm^{-1} range is reported. Binding of CO to the reduced enzyme gives two heme(II)−CO ν_{C-O} stretches (1927 and 1904 cm^{-1}) which appear to be in rapid equilibrium. Photolysis of this heme(II)−CO compound is accompanied by perturbation of the local fine structure around the catalytic site giving vibrational changes of protein backbone, substrate, amino acid residues, and cofactors, to which heme, substrate arginine, and catalytic site residues contribute. Possible assignments of vibrations to heme, substrate arginine, and catalytic site residues are discussed. The discussion of assignments is informed by known structures, absorbance frequencies, and extinction coefficients of residues and cofactors, analysis of H_2O-D_2O exchange effects, analysis of substrate $^{14}N-^{15}N$ (guanidinium)−arginine exchange effects, and comparison with the nNOS isoform (which differs in the replacement of asparagine 368 with an aspartate within the substrate binding site). The FTIR data can be modeled on the known structure of the catalytic site and indicate the extent of modulation of vibrational modes upon photolysis of the CO compound.

Nitric oxide synthases (NOSs)[1] are widely distributed, and NO is a ubiquitous cell-signaling molecule with central roles in physiology and pathology (*1*−*7*). NO is produced by NOS from arginine by a two-step NADPH and O_2-dependent oxidation to citrulline (*8*−*11*). The three mammalian isoforms of NOS are regulated differently; the neuronal and endothelial isoforms (nNOS and eNOS, respectively) are regulated by Ca^{2+}-calmodulin, while the cytokine inducible isoform (iNOS) is constitutively active. The active forms of all three are homodimers and consist of an N-terminal oxygenase domain and a C-terminal multidomain reductase linked by a calmodulin-binding site (*12*). The oxygenase domain contains iron−protoporphyrin IX (heme B) and tetrahydrobiopterin (H_4B) prosthetic groups; this region comprises the catalytic core of the molecule (*13*, *14*). The reductase domains contain FMN, FAD, and the NADPH binding site (*15*).

The NOS oxygenase domains form a distinct family, members of which are not closely related to other enzymes, and are not homologous to the members of the cytochrome P450 superfamily which has a superficially similar heme−thiolate site for oxygen chemistry. The reductase domains, in contrast, are closely related to cytochrome P-450 reductases (*16*). Crystal structures of the NOS oxygenase domain have been determined (*17*−*20*). From these structures, the residues involved in L-arginine binding have been identified, but the reaction mechanism is not fully resolved. The catalytic site has recently been probed further by resonance Raman spectroscopy (*21*, *22*) and by Fourier transform infrared spectroscopy (FTIR) (*23*, *24*). Resonance Raman spectroscopy has shown that hydrogen bonding between the proximal cysteine and a tryptophan residue modulates the strength of the $Fe^{III}-NO$ bond (*21*, *22*). FTIR studies on nNOS, utilizing heme(II)−CO photolysis to specifically probe the catalytic site, have identified multiple CO binding modes and discussed possible assignments of some vibrational bands of prosthetic groups, ligands, and amino acid residues (*24*).

Improvements in sensitivity and data processing of FTIR spectroscopy enable the technique to be used to detect changes in protein structure at the atomic level. In this study, photolysis of the CO adduct of ferrous eNOS is used to obtain difference spectra of a limited subset of vibrations that are perturbed by these changes at the catalytic site. This technique has also been applied to other five-coordinate hemoproteins, including cytochrome *c* oxidase, nNOS, myoglobin, and cytochrome bo_3 (*24*−*30*). We report CO photolysis studies on the full-length eNOS (MW = 133 kDa)

† This work was funded by grants from The Nuffield Foundation (W.J.I.), The Wellcome Trust (Grant 049722, to P.R.R.), and The American Diabetes Association (S.M.E.S. and J.C.S.).

* To whom correspondence should be addressed: Biomolecular Sciences Building, School of Biology, University of St. Andrews, St. Andrews KY16 9JF, U.K. Phone: (44) 1334 463408. Fax: (44) 1334 463400. E-mail: wji@st-andrews.ac.uk.

‡ University of St. Andrews.

§ Rensselaer Polytechnic Institute.

|| University College London.

[1] Abbreviations: FTIR, Fourier transform infrared; ATR, attenuated total reflectance; NOS, nitric oxide synthase; nNOS, neuronal nitric oxide synthase; eNOS, epithelial nitric oxide synthase; iNOS, cytokine inducible nitric oxide synthase; NO, nitric oxide; CO, carbon monoxide; H_4B, tetrahydrobiopterin.

10.1021/bi047891y CCC: $30.25
Published on Web 02/19/2005

in the 1000−2500 cm^{-1} region where vibrational bands of ligands, prosthetic groups, proteins, and amino acid side chains are found. Provisional assignments of vibrations are made on the basis of spectra of model compounds, stable isotope effects (deuterium and ^{15}N), comparison with FTIR data on the related nNOS isoform, and a knowledge of NOS atomic structures.

MATERIALS AND METHODS

NOS Purification. Bovine endothelial nitric oxide synthase (eNOS) was purified from protease-deficient *Escherichia coli* strain ER2556 transformed with pGROELS and the pCWori+ eNOS vector as described previously (*31*). Cells expressing eNOS were broken using a French pressure cell (7000 psi). After cell fragments had been removed by ultracentrifugation for 70 min at 144000*g*, eNOS was purified from the supernatant by 2′−5′ ADP Sepharose affinity chromatography. The enzyme was concentrated to approximately 30 μM and stored at −80 °C in 50 mM Tris buffer (pH 7.4), 0.1 mM dithiothreitol, 0.1 mM EDTA, 500 mM NaCl, 1 mM H_4B, and 2 mM arginine with 10% glycerol. Activity was assessed using the Greiss assay in a 96-well plate format (*32*). The heme content, the integrity of thiolate ligation, and the ability to bind arginine were assessed spectrophotometrically by monitoring the formation of the characteristic optical 450 nm and the infrared 1927 and 1904 cm^{-1} bands of the ferrous−CO liganded form of the enzyme (*24*).

Preparation of FTIR Samples. The heme and H_4B replete eNOS was dialyzed into a buffer of 40 mM TES, 20 mM arginine, 2 mM EDTA, 1 mM dithiothreitol, 0.1 mM $CaCl_2$, 1 μM H_4B, and 1% glycerol (pH 7.6) and concentrated using centrifugal concentrators (Vivascience Ltd., Lincoln, U.K.). An enzyme solution (10 μL) containing approximately 8 nmol of eNOS was pipetted onto a 25 mm diameter CaF_2 window and placed under a stream of water-saturated CO gas. The sample was then reduced with 2.0 μL of 0.1 M sodium dithionite [in 400 mM TES, 100 mM arginine (pH 7.6), and 10% glycerol]. After further exposure to the stream of CO for 1 min, a second CaF_2 window was placed on top, the sample was squeezed to an optimal thickness, and the edges were sealed with Dow Corning MS24 Silicon Compound. Formation of the reduced CO compound was confirmed by detection of characteristic Soret and visible bands and by observation of the characteristic heme(II)−CO bands at 1927 and 1904 cm^{-1} in the absolute FTIR spectrum.

D_2O Exchange. The eNOS to be exchanged into D_2O was diluted 10-fold in 40 mM TES, 20 mM arginine, 2 mM EDTA, 1 mM dithiothreitol, 0.1 mM $CaCl_2$, 1 μM H_4B, and 1% glycerol (pD 7.6) in D_2O and reconcentrated using Vivascience centrifugal concentrators. This process was repeated three times. Samples were then prepared as for H_2O solutions, but with all re-wetting solutions prepared with equivalent D_2O buffers and with a CO stream saturated with D_2O vapor. The pD was measured by a pH electrode using the relation pD = pH reading + 0.4 (*34*). The extent of H−D exchange was estimated using the amide II region of the absolute spectra following published methods (*33*, *35*). The amide II band is 60% due to N−H bending (40% C−N stretch) which shifts from 1545 to 1445 cm^{-1} upon deuteration. In the preparation used here, the extent of H−D exchange was >85%.

FTIR Photolysis Difference Spectroscopy. FTIR spectra were recorded on a Brüker ISF 66/S spectrometer fitted with a liquid nitrogen-cooled MCT-A detector. Actinic light was provided by a 250 W quartz−iodine lamp, filtered with glass heat filters, water, and BG39 filters, and delivered to the sample via a light pipe. The sample was water-thermostated at 283 K. Typically, 100 interferograms at 4 cm^{-1} resolution were averaged to provide an initial dark baseline; the light was then switched on, and the recording was repeated after a delay of 1 s. Finally, the light was switched off and the recording repeated after dark relaxation for 2 s to provide an indication of relaxation rate and sample baseline drift (*25*). Light−dark cycles were repeated up to 5000 times over periods of up to 3 days to enable signals of 10^{-6} ΔA to be observed reliably. All frequencies are accurate to ± 1 cm^{-1}. The enzyme is stable under these conditions over this period [nNOS under similar conditions slowly converts to the inactive P420 form (*24*)]. Unless otherwise stated, spectra are unligated (i.e., light) minus ligated (i.e., dark) difference spectra from which 50% of the final dark baseline drift (i.e., final dark recording minus initial dark recording) has been subtracted. Visible absorbance spectra of the samples in the CaF_2 windows were obtained to monitor integrity.

The kinetics of CO recombination and the accompanying relaxation of vibrational states were assessed by averaging together batches of interferograms at various times after switching off illumination with a fast photographic shutter (Figure 1).

Spectra of Model Compounds. Vibrational spectra of [^{14}N]-L-arginine (natural abundance) and [^{15}N](guanidinium)-L-arginine in H_2O and D_2O were obtained from 100 mM solutions (adjusted to pH/pD 7.6) of the amino acid by attenuated total reflectance (ATR) FTIR by placing the sample solution on the surface of the internally reflecting quartz prism.

RESULTS

CO Photolysis Difference Spectra: the Heme−CO Stretch. The inset spectra in Figure 1 show the CO photolysis difference spectrum and the inverted absolute spectrum of the heme(II)−CO stretch of eNOS in H_2O. The photolysis difference spectrum (Figure 1, inset trace A) has been expanded 8-fold with respect to the absolute spectrum. The absolute spectrum (inverted for ease of comparison) of the heme(II)−CO compound (Figure 1, inset trace B) has a buffer blank subtracted and a background ramp correction applied. The relative magnitudes of the two spectra show that there is an approximately 12% steady state level of heme(II)−CO photolyzed under illumination. The ratios of CO bands in the photolysis spectra will be influenced by the kinetics of CO recombination, the light intensity, and the quantum yield of CO photolysis. However, a comparison of the heme(II)−CO ν_{C-O} stretch in the absolute spectra and the photolysis spectra shows only a marginally different ratio of the principal heme(II)−CO photolysis bands at 1927 and 1904 cm^{-1}, the 1904 cm^{-1} species being slightly more prominent in the photolysis spectra. The absolute heme(II)−CO stretches can be best fitted by Gaussian distributions at 1927.9 cm^{-1} [bandwidth at half-height ($\Delta\nu_{1/2}$) of 20.8 cm^{-1}]

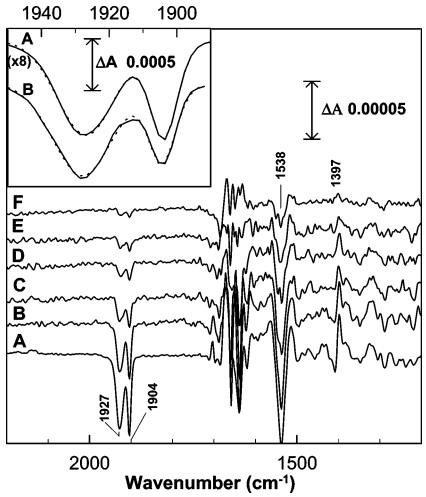

FIGURE 1: FTIR spectra of the absolute and CO photolysis difference spectrum of the heme−CO adduct (inset) and time dependence of the relaxation of the light-induced FTIR difference spectra of CO photolysis in H_2O. Spectra of the heme−CO adduct are given in the inset. (A) Photolysis difference spectrum. The spectrum shown is the light minus dark difference spectrum (8-fold). The magnitude of the photolysis difference spectrum is approximately an eighth of that of the absolute spectrum. The dashed line is the simulated spectrum (see the text). (B) Background-corrected absolute spectrum of the ferrous heme−CO stretch. The spectrum was obtained by subtracting a buffer blank from the absolute FTIR spectrum of the eNOS−CO compound. A ramp correction was also used and the spectrum inverted for ease of comparison. The dashed line is the simulated spectrum (see the text). Time lapse spectra are given in the main panel. Difference spectra were taken at times during or following the end of illumination: (A) under illumination, (B) difference spectrum within 400 ms of illumination, (C) spectrum from 400 ms to 1.2 s post-illumination, (D) spectrum from 1.2 to 2.0 s post-illumination, (E) spectrum from 2.0 to 2.8 s post-illumination, and (F) spectrum from 2.8 to 4.6 s post-illumination. The samples were prepared and spectra obtained as described in Materials and Methods.

and 1904.4 cm^{-1} ($\Delta\nu_{1/2}$ = 9.5 cm^{-1}); in the photolysis difference spectrum, the equivalent bands can be fitted by 1926.9 cm^{-1} ($\Delta\nu_{1/2}$ = 20.1 cm^{-1}) and 1903.9 cm^{-1} ($\Delta\nu_{1/2}$ = 9.7 cm^{-1}) (dashed lines in Figure 1 inset). There are small residuals in the fits which may indicate small amounts of alternative forms, as seen in other hemoproteins (*24*−*30*, *36*). The residuals may also lead to the slight differences in frequency between the absorbance and photolysis spectra, which we do not consider significant. The equivalent Guassian fittings for the heme(II)−CO stretch in D_2O (not shown) gave values of 1925.9 cm^{-1} [bandwidth at half-height ($\Delta\nu_{1/2}$) of 20.8 cm^{-1}] and 1903.1 cm^{-1} ($\Delta\nu_{1/2}$ = 9.7 cm^{-1}) for the absolute spectrum and 1925.8 cm^{-1} ($\Delta\nu_{1/2}$ = 20.3 cm^{-1}) and 1902.8 cm^{-1} ($\Delta\nu_{1/2}$ = 10.1 cm^{-1}) for the photolysis difference spectrum. The ratio of the areas under the two components in the photolysis difference spectrum is approximately 2:1 (64% vs 36%), and this ratio remained constant for many samples and several preparations. In the CO photolysis spectra of nNOS (*24*), we reported features associated with the ν_{C-O} of the inactive P420 form, in which the heme has lost its axial thiolate ligand. The spectra of eNOS (in the presence of arginine and H_4B) show no indication of formation of the P420 form, although this species is formed in the absence of arginine in both eNOS and nNOS.

Postphotolysis Relaxation Kinetics. Difference spectra taken at different time intervals following the relaxation of the photolyzed CO compound after switching the light off are shown in Figure 1. The two heme(II)−CO species recombine at the same rate, and all other major features relax roughly in parallel with the heme(II)−CO recombination. Data for postphotolysis CO recombination kinetics are not available for eNOS, but optically monitored kinetic analyses for the postphotolysis recombination of CO with nNOS have been published (*37*). In nNOS replete with L-arginine and H_4B, more than 95% of the recombination occurs in a single slow phase with a recombination rate of 2×10^4 M^{-1} s^{-1} at 300 K (*37*). Herein we observe a pseudo-first-order rate constant of approximately 2 s^{-1} at the lower temperature of 283 K. If one allows for the lower temperature used herein, the kinetics are roughly comparable to those of nNOS, which gives results broadly similar to those for nNOS for the photolysis FTIR difference spectra (*24*). This slow phase will incorporate the changes we see in the FTIR; the small fraction of faster recombination phases, if they occur in eNOS, would be too rapid to be observable in our FTIR experiments.

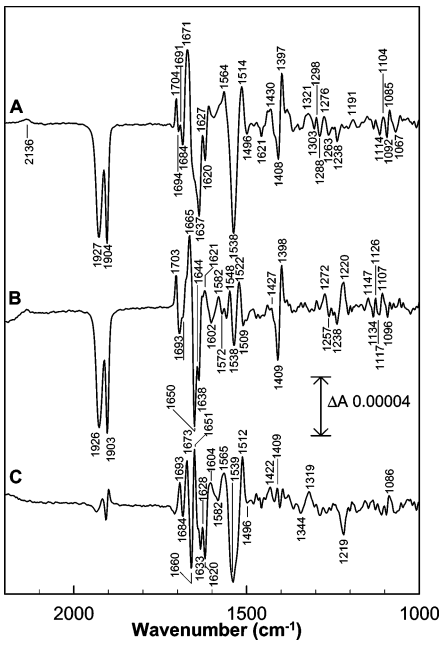

FIGURE 2: Light-induced FTIR difference spectra of eNOS due to CO photolysis (H_2O and D_2O). (A) Light minus dark difference spectra in H_2O media. (B) Light minus dark difference spectra in D_2O media. (C) Double difference spectrum of the spectrum in H_2O (trace A) minus the spectrum in D_2O (trace B). The CO photolysis spectra are averages of 2000 scans, each scan consisting of 100 averaged interferograms at 4 cm^{-1}. Photolysis is by a 250 W lamp protected by BG39 and water filters. All spectra were obtained at 283 K. Samples of the CO adduct of fully reduced eNOS were prepared in H_2O buffers at pH or pD 7.6 as described in Materials and Methods. After sufficient time for equilibration and settling at 283 K, repetitive light−dark cycles were recorded and averaged. The light minus dark spectra (traces A and B) have 50% of the dark minus dark control subtracted, although this made no significant difference to the trace.

CO Photolysis Difference Spectra: Protein and Cofactor Vibrations. Figure 2A shows a static heme(II)−CO photolysis difference spectrum of eNOS in H_2O at pH 7.6 and 283 K in the 1000−2400 cm^{-1} range. A 50% weighted difference spectrum of dark (pre-illumination) minus dark (post-illumination) has been subtracted to remove any baseline drift, although this had very little effect on the resultant spectra (not shown). Positive peaks correspond to features

Table 1: Principal Spectral Features in the Photolysis Difference Spectra[a]

H_2O		D_2O				
peak	trough	peak	trough	heme	vibrations which may occur at these frequencies	
	1927		*1926*		heme(II)−CO stretch	
	1904		*1903*		heme(II)−CO stretch	
1704	1694	*1703*	*1693*	*b*	heme propionate	
1671						amide I region
1627	1637				ν_s guanidinium	amide I region
		1665	*1650*			*amide I region*
		1644	*1638*			*amide I region*
		1621	*1602*		*ν_{as} guanidinium*	*ν_{as} carboxylate*
	1620					
		1582	*1572*		*ν_s guanidinium*	
1564					ν_{as} carboxylate	amide II region
	1538	*1548*	*1538*	*b*	ν(C*b*C*b*) heme	amide II region
1514	1496	*1522*	*1509*			tyrosine ν(CC) ring?
1430	1408	*1427*	*1409*		ν_s carboxylate	
1397		*1398*		*c*	ν(CN) asparagine	ν(C*a*N) heme
1321	1303				NH_3^+ arginine	
1298	1288					
1276	1263	*1272*	*1257*		tyrosine ν(CO), ν(CC)	
	1238		*1238*	*b*		δ(C*m*H) heme
		1220			*δNH_3^+ arginine*	
		1147	*1134*			
	1114	*1126*	*1117*			
1104	1092	*1107*	*1096*			tryptophan?
1085	1067					tryptophan?

[a] D_2O data and assignments are in italics. [b] Similar "heme" vibration observed in the CO photolysis spectra of nNOS, horseradish peroxidase, or cytochrome *c* oxidase. [c] Similar "heme" vibration observed in the CO photolysis spectra of only horseradish peroxidase.

generated in the photodissociated enzyme and troughs due to those lost on photolysis of the CO-bound enzyme. The changes caused by photolysis of the heme-bound CO ligand can be seen as troughs at 1927 and 1904 cm^{-1} as discussed above. Putative "B-states" of the CO-ligated form (*36*) are observed weakly at 2136 cm^{-1}. Features in the photolysis difference spectra arise from a limited subset of residues which are significantly affected by CO binding. The spectra from 1000 to 1800 cm^{-1} contain changes in vibrational transitions associated with the protein backbone (amide I and II), substrate, prosthetic groups, and amino acid residues. The major peaks and troughs are marked on the spectra in Figure 2 and listed in Table 1. The guanidinium ν_{as} of the substrate arginine bound to eNOS probably shows in the photolysis spectra of eNOS; in the vibration at 1691/1684 cm^{-1} (Figure 2A), this shifts to 1621/1602 cm^{-1} in D_2O (Figure 2B) (*40*, *41*, *48*). Strong differences at 1693/1684 and 1620/1604 cm^{-1} in the H_2O minus D_2O double difference spectrum further support these assignments (Figure 2C). The guanidinium ν_s is expected around 1634 cm^{-1} in H_2O and 1586 cm^{-1} in D_2O.

A Comparison of Vibration Spectra in H_2O and D_2O Media. Shown in Figure 2B is a heme(II)−CO photolysis difference spectrum of eNOS in D_2O at pD 7.6 and 283 K. A 50% weighted difference spectrum of dark (pre-illumination) minus dark (post-illumination) has been subtracted to remove any baseline drift, although this had very little effect on the resultant spectra (not shown). The main features of the eNOS D_2O spectrum are listed in Table 1. Figure 2C is the double difference spectrum of the D_2O photolysis difference spectrum minus the H_2O photolysis difference spectrum where major differences due to isotopic exchange become more apparent. The differences observed around 1927−1903 cm^{-1} are due to the small isotope-induced shifts in the heme(II)−CO stretches; absorbances at lower frequencies are due to cofactor, ligand, and residue vibrations that shift upon H−D exchange. The effects of the isotope exchange assist in the assignment of vibrations. A prominent difference is observed at 1693/1684 cm^{-1} which may be due to a shift in the ν_{as} of the guanidinium group on deutration; this is followed by a complex series of differences in the amide I region, followed by a large difference at 1539 cm^{-1} probably incorporating amide II band contributions which shift upon deuteration.

As stated above, the guanidinium ν_{as} of the substrate arginine probably appears at 1691/1684 cm^{-1} in Figure 2A (H_2O), and shifts to the region of 1621/1602 cm^{-1} in D_2O (Figure 2B); this would show in the double difference spectrum (Figure 2C; 1693/1684 and 1620/1604 cm^{-1}) (*40*, *41*, *48*). In the double difference spectrum, the vibrational differences which are not H/D sensitive are canceled but those which are occur twice (in the H_2O position and inverted in the D_2O position).

A Comparison of the FTIR Heme(II)−CO Photolysis Spectra of eNOS with [^{15}N](Guanidinium)-Arginine and [^{14}N]Arginine. Replacement of the ^{14}N isotope with the ^{15}N isotope in the guanidinium moiety affects its vibrational frequencies. Shown in Figure 3 are ATR-FTIR spectra of L-arginine and [^{15}N](guanidinium)-L-arginine in H_2O and D_2O. The difference spectra and fitting the areas under the curves in the light of published parameters (*40*, *41*) indicate the guanidinium ν_{as} shifts from approximately 1673 to 1658 cm^{-1} on ^{15}N substitution in H_2O and from approximately 1617 to 1607 cm^{-1} in D_2O. The guanidinium ν_s shifts from approximately 1635 to 1623 cm^{-1} on ^{15}N substitution in H_2O and from approximately 1586 to 1574 cm^{-1} in D_2O. The arginine carboxylate is reported to have a ν_{as} in H_2O of ~1595 cm^{-1} (460 M^{-1} cm^{-1}) and a ν_s at 1414 cm^{-1} (~300 M^{-1} cm^{-1}) [in D_2O, 1590 cm^{-1} (~800 M^{-1} cm^{-1}) and 1411 cm^{-1} (~350 M^{-1} cm^{-1}), respectively]. The amino group has

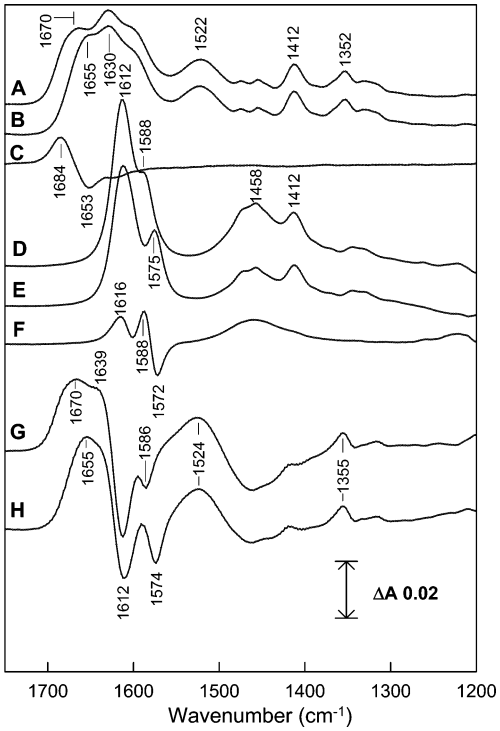

FIGURE 3: ATR FTIR spectra of [^{14}N]-L-arginine and [^{15}N](guanidinium)-L-arginine at pH 7.6 and pD 7.6. The absolute spectra of 100 mM L-arginine are shown: (A) [^{14}N]-L-arginine at pH 7.6, (B) [^{15}N](guanidinium)-L-arginine at pH 7.6, (C) difference between spectrum A and spectrum B (the ^{14}N−^{15}N difference spectrum in H_2O), (D) [^{14}N]-L-arginine at pD 7.6, (E) [^{15}N](guanidinium)-L-arginine at pH 7.6, (F) difference between spectrum D and spectrum E at pD 7.6 (the ^{14}N−^{15}N difference spectrum in D_2O), (G) H−D isotopic difference spectra for [^{14}N]arginine (A minus D), and (H) H−D isotopic difference spectra for [^{15}N](guanidinium)-arginine (B minus E). The spectra were obtained at 293 K using a quartz ATR prism.

a δ_{as} in H_2O at 1630 cm^{-1} (200 M^{-1} cm^{-1}) and a δ_s at 1518 cm^{-1} (180 M^{-1} cm^{-1}); in D_2O, the δ_{as} shifts to approximately 1176 cm^{-1} and the δ_s to below 1000 cm^{-1}. In the H_2O spectra (Figure 3A,B), there is a vibration around 1350 cm^{-1} which, being D_2O sensitive and present in all amino acid spectra, can be assigned to another vibrational mode of NH_3^+. The frequencies of absorbance maxima may be shifted, and line widths are likely to be narrower under the constraints imposed when the arginine is bound to the enzyme.

A comparison of the photolysis difference spectra, when [^{15}N](guanidinium)-L-arginine or [^{14}N]-L-arginine is bound at the catalytic site, allows firm identification of the arginine guanidinium ν_{as} and ν_s vibrations. Photolysis difference spectra of eNOS with [^{15}N](guanidinium)-L-arginine bound are shown in Figure 4 (H_2O) and Figure 5 (D_2O) with their respective ^{14}N−^{15}N isotopic double difference spectra (B). As can be seen from these double difference spectra, the [^{15}N](guanidinium)-L-arginine substitution elicits changes in the FTIR photolysis difference spectra, and this difference is used to assist in making assignments to the guanidinium moiety and its immediate neighbors. In Figure 4A, the ν_{as} of the [^{15}N]guanidinium would be expected to contribute to the large 1667/1649 cm^{-1} feature. In the ^{14}N−^{15}N double difference spectrum (Figure 4B), the guanidinium ^{14}N ν_{as} and ^{15}N ν_{as} differences may be seen at 1696/1687 and 1676/1659 cm^{-1}, respectively. The guanidinium ^{14}N ν_s and ^{15}N ν_s may be seen in the double difference spectra at 1647/1636

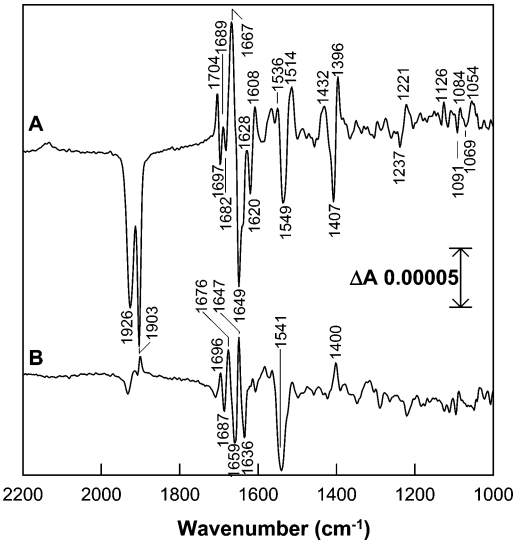

FIGURE 4: Comparison of the light-induced CO photolysis FTIR difference spectra of eNOS with [^{15}N](guanidinium)-L-arginine in H_2O. (A) eNOS FTIR heme(II)−CO photolysis difference spectrum obtained under the same conditions as in Figure 2A (H_2O) but with [^{15}N](guanidinium)-L-arginine bound instead of the naturally occurring isotope. (B) Double difference spectrum between the photolysis difference spectra of the [^{14}N]- and [^{15}N]arginine ligated forms (spectrum in Figure 2A minus spectrum A). Experimental and spectrometer conditions are as described in the legend of Figure 2. The spectra were normalized prior to subtraction on the estimated area under the heme(II)−CO photolysis component.

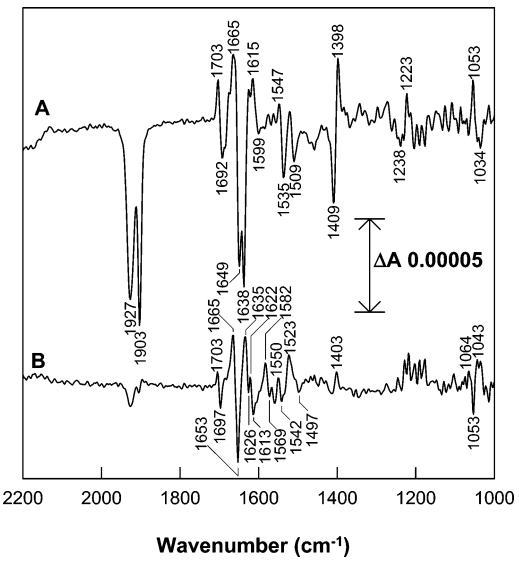

FIGURE 5: Comparison of the light-induced CO photolysis FTIR difference spectra of eNOS with [^{15}N](guanidinium)-L-arginine in D_2O. (A) eNOS FTIR heme(II)−CO photolysis difference spectrum obtained under the same conditions as in Figure 2B (D_2O) but with [^{15}N](guanidinium)-L-arginine bound instead of the naturally occurring isotope. (B) Double difference spectrum between the photolysis difference spectra of the [^{14}N]- and [^{15}N]arginine ligated forms (spectrum in Figure 2B minus spectrum A). The spectra were normalized prior to subtraction on the estimated area under the heme(II)−CO photolysis component. Experimental and spectrometer conditions were as described in the legend of Figure 2.

cm^{-1}. Also included in this region (~1650 cm^{-1}) will be any contribution from the backbone carbonyl which is H-bonded to the guanidinium. The trough at 1541 cm^{-1} is in part due to the amide II band in balance between the subtracted spectra. The difference in vibration seen at 1400 cm^{-1} in Figure 4B is probably due to the ν_s of the carboxylate

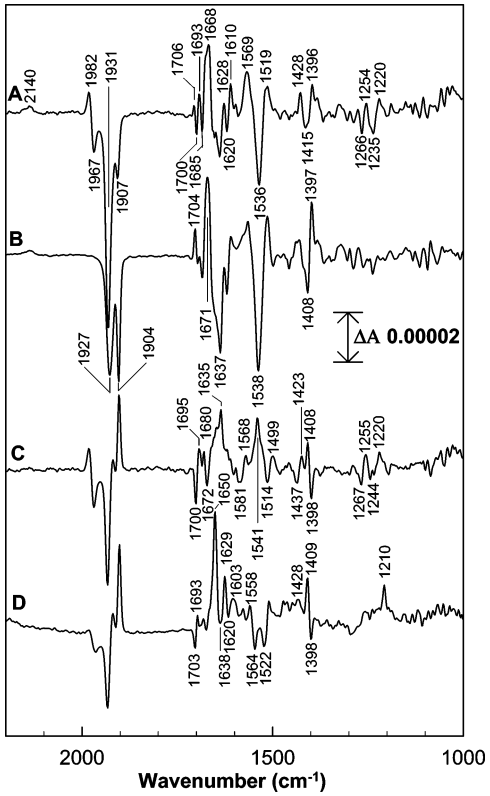

FIGURE 6: Comparison of the light-induced CO photolysis FTIR difference spectra of eNOS and nNOS in H_2O and D_2O. (A) nNOS FTIR photolysis difference spectrum in H_2O from ref *24*, and obtained under the same conditions as in Figure 2. (B) eNOS FTIR photolysis difference spectrum in H_2O (as in Figure 2A). (C) Double difference spectrum (spectrum A minus spectrum B). (D) Double difference spectrum of nNOS photolysis difference spectrum and eNOS photolysis difference spectrum in D_2O (parent spectra from ref *24* and Figure 2B). The double difference spectra were obtained by subtracting the eNOS spectra from the corresponding nNOS spectra after scaling. The eNOS spectra are taken from Figure 2 and the nNOS spectra from our previous work (*24*).

of the glutamate (E363) residue which is H-bonded to the guanidinium. In the double difference spectrum in Figure 5B (D_2O media), the resolution of the spectrum is more difficult because there is greater overlap between the species. The guanidinium ν_{as} should contribute two peaks and troughs (one pair corresponding to the ^{14}N vibration and one to the ^{15}N vibration) between 1635 and 1600 cm^{-1}. The guanidinium ν_s will similarly contribute between 1600 and 1565 cm^{-1}, close to any contributions from the glutamate carboxylate ν_{as}. The difference at 1665/1653 cm^{-1} could be due to a peptide carbonyl (trytophan, W358, Figure 7) to which the guanidinium group is H-bonded. The subtraction of the heme(II)−CO ν_{C-O} spectra ($^{14}N-^{15}N$) leaves residual differences (Figure 4B) similar to those observed in the H−D difference spectra (Figure 2C) and attributable to a small shift caused by the ^{14}N or ^{15}N substitution.

A Comparison of the FTIR Heme(II)−CO Photolysis Spectra of eNOS and nNOS. The FTIR difference spectra of nNOS and eNOS are compared in parts A and B of Figure 6. The difference between these spectra is trace C, and trace D shows the equivalent double difference spectra obtained in D_2O media. In eNOS, asparagine N368 is H-bonded to the carboxylate of the substrate arginine; in nNOS, this position is occupied by an aspartate, representing the only residue replacement in the immediate substrate binding network of the two isoforms. Thus, a comparison of the photolysis difference spectra of the two isoforms may be instructive. In traces C and D, features which correspond to the differences in the H-bond network between the two isoforms are seen. Principle among these will be vibrations of asparagine which are expected at 1668 cm^{-1} [ν(C═O), $\epsilon \sim 320$ M^{-1} cm^{-1}], 1612−1622 cm^{-1} [$\delta(NH_2)$, $\epsilon \sim 150$ M^{-1} cm^{-1}], and 1410 cm^{-1} [ν(CN)] in H_2O (1650, 1163, and 1409 cm^{-1} in D_2O, respectively) (*40*, *47*) and of the aspartate which replaces it. Thus, the sharp feature at 1408/1398 cm^{-1}, which can be assigned to ν(CN), is underlaid by a broader feature (1423 cm^{-1}) that can be assigned to ν_s of COO^-, probably that of the replacement aspartate. As is apparent in Figure 7, other differences are expected in the H-bond network in the two isoforms, and these will also contribute to the double difference spectra.

DISCUSSION

Photolysis of the heme(II)−CO compound will perturb the dynamic structure in its local environment. The arginine bound at the catalytic site will reorient; conflict between the arginine and CO binding has been reported [the presence of arginine slows CO recombination by orders of magnitude (*38*), and conversely CO increases the K_d for arginine (*39*)]. It is probable that on photolysis the arginine relaxes into a preferred binding mode, hence slowing the recombination of CO. On the proximal side of the heme, the thiolate ligand moves as the iron moves out of the heme plane on photolysis of the CO compound. Resonance Raman spectroscopy has shown that hydrogen bonding between the proximal cysteine and a tryptophan residue modulates the strength of the heme(III)−NO bond (*21*, *22*). The substrate−arginine H-bonding network is indicated from crystallographic studies; the guanidinium is H-bonded to the carboxylate of glutamate (E363) and the backbone peptide O of tryptophan (W358) (*17*−*20*). The substrate−arginine NH_3^+ group appears to be H-bonded to the heme propionate and also to the carboxylate of glutamate (E363). The substrate−arginine carboxylate appears to be H-bonded to the NH_2 group of glutamine (Q248) and asparagine (N368) (this latter is replaced with an aspartate in nNOS and iNOS), and tyrosine OH (Y358). In the next sphere, H_4B is bonded through the heme propionate (*17*−*20*). This network is illustrated in Figure 7, which shows views of the heme and arginine binding sites of nNOS and eNOS (iNOS is similar to nNOS).

Heme(II)−CO Stretch. The heme(II)−CO photolysis spectra are shown inset in Figure 1; there are two minima (1927 and 1904 cm^{-1}). The ratio of these two components is constant between samples and probably represents two modes of binding in rapid equilibrium, the narrower band, corresponding to ~36% of the area under the absorbance curve, representing a more constrained configuration. A comparison with the two other mammalian isoforms, nNOS and iNOS, is interesting; all three isoforms appear to exhibit two bands, but the relative ratios of the bands are different. In nNOS, two similar modes are observed at 1931 cm^{-1} [half-height bandwidth ($\Delta\nu_{1/2}$) of 15.4 cm^{-1}] and 1907 cm^{-1} ($\Delta\nu_{1/2}$ = 10.7 cm^{-1}) (*24*); however, the component at 1907 cm^{-1} is smaller, and the higher-frequency component is responsible for nearly 80% of the area under the absorption peak. In iNOS, the situation is reversed; the dominant species, under comparable conditions, is at 1905 cm^{-1} ($\Delta\nu_{1/2} = 9.5$ cm^{-1}),

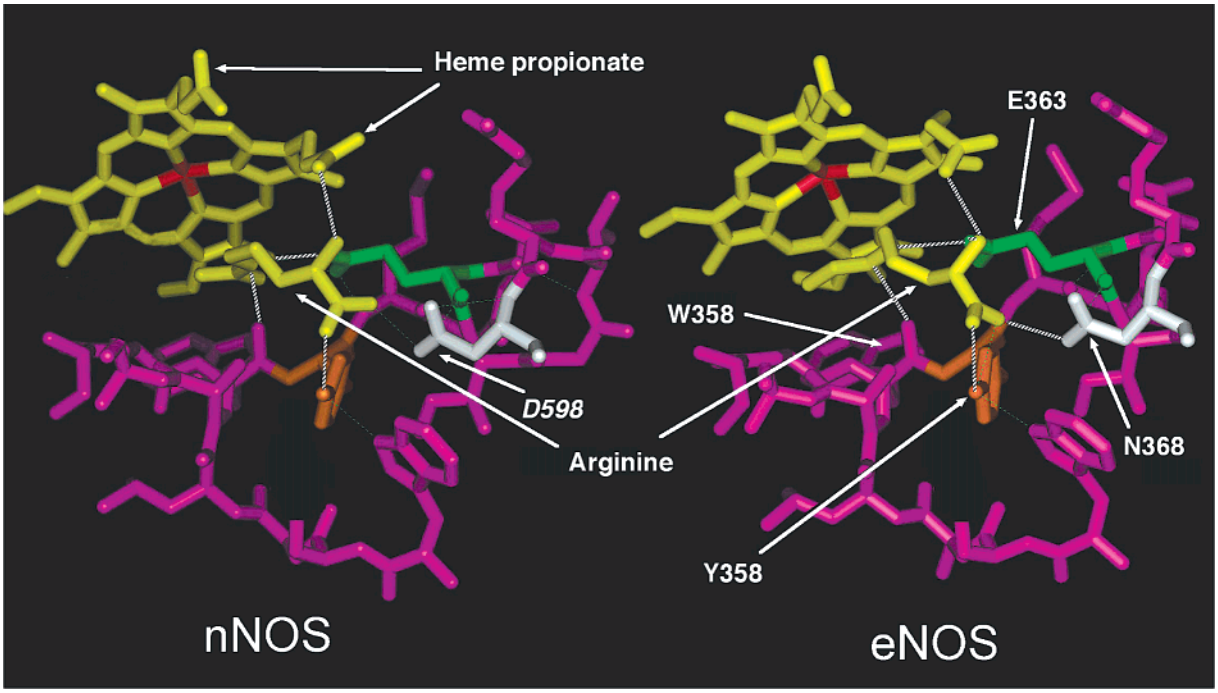

FIGURE 7: Model of the active site and H-bonding network. Views of the heme and arginine binding sites of nNOS and eNOS. Heme is colored yellow, and the Fe atom is colored red. Arginine (nNOS) and N−OH arginine (eNOS) are colored yellow. Key binding site residues indicated by color are as follows: E592 (nNOS) and E363 (eNOS) in green, D592 (nNOS) and N368 (eNOS) in white, and Y588 (nNOS) and Y358 (eNOS) in orange. Structures are in the CO free state as shown. The lack of conservation at the D592/N368 position affects the ligand geometry and H-bonding pattern in this region. The pdb files are (A) 1OM4 (structure of rat neuronal nitric oxide synthase heme domain with L-arginine bound, deposited by H. Li, P. Martasek, H. Shimizu, B. S. S. Masters, T. L. Poulos, and C. S. Raman) and (B) 5NSE (bovine endothelial nitric oxide synthase heme domain, with hydroxyarginine bound, deposited by C. S. Raman, H. Li, P. Martasek, B. S. S. Masters, and T. L. Poulos).

with only a minor component indicated at a higher frequency (*36*). The simplest interpretation of the spectra is that two similar principle states exist in all three isoforms and that the proportional occupancy of each state is different in each of the three isoforms. The ν_{C-O} stretches of different hemoproteins have characteristic frequencies between 1904 and 1970 cm^{-1} with $\Delta\nu_{1/2}$ between 5 and 15.4 cm^{-1}; multiple peaks are commonly observed (*24*−*30*, *36*, *42*, *43*). Thus eNOS is exceptional: the 1904 cm^{-1} species is at the low end of the frequency range and the 1927 cm^{-1} species when $\Delta\nu_{1/2} = 20.8$ cm^{-1} is broader than previously studied heme−CO compounds. The highest bandwidth reported previously, 15.4 cm^{-1}, was observed in the nNOS isoform (*24*); this tendency may be the result of the unusually open pocket composed of β-sheet folds, rather than tightly packed α-helices. Both polarization of the CO molecule at the heme and bending of the heme−CO compound by steric interactions influence the position of the absorption. In general, hydrogen bonding of the CO to groups, including arginine, in the heme pocket would result in a lowering of the stretching frequency, while contact with nonpolar residues would increase it (*27*). The simplest explanation is that the CO in the 1904 cm^{-1} species is more strongly H-bonded than that in the 1927 cm^{-1} species, water and the guanidinium moiety being the most likely partners.

All three isoforms of NOS show a putative B-form of the ν_{CO} stretch around 2140 cm^{-1} (*24*, *36*). This is seen in Figure 2 for eNOS (2136 cm^{-1}). These B-states in iNOS have been discussed by Jung and co-workers (*36*), who suggest, by analogy with myoglobin, that this state represents CO adjacent to the heme and almost parallel to the heme plane after photolysis. The B-state is observed in photolysis spectra of other hemoproteins, cytochrome *c* oxidase and homologues, all three isoforms of NOS, and horseradish peroxidase. In cytochrome *c* oxidase, it is assigned to CO ligation to an intrinsic copper ion, but the other enzymes lack any additional intrinsic transition metal (*30*, *41*; W. J. Ingledew and P. R. Rich, unpublished observations on horseradish peroxidase).

Protein, Residue, Cofactor, and Ligand Vibrations. The spectral range from 1000 to 1700 cm^{-1} encompasses many vibrations due to the protein backbone, amino acid residues, cofactors, and ligands. The region around 1653 cm^{-1} in absolute spectra (not shown) is dominated by the amide I band which is due to vibrations of the protein backbone (80% due to C═O stretching, 10% to C−N stretching, and 10% to N−H bending). The amide I region also contains many other vibrations such as contributions from amino acid residues. Around 1550−1510 cm^{-1} in absolute spectra is the amide II band; this is 60% due to N−H bending and 40% due to C−N stretching. The N−H absorbance shifts in D_2O. In the absolute spectra, the absorbance is approximately 10^4 times greater in these regions than in the photolysis difference spectra shown here. At frequencies below the amide II band, further residue, ligand, and cofactor vibrations occur.

Heme IX. Changes in vibrations associated with the heme group upon photolysis of its Fe^{II}−CO adduct are expected. However, aside from the assignments for propionic acid groups, there are few satisfactory model compounds available to assist in the assignments for the high-spin NOS heme vibrations. Vibrations of reduced low-spin ferrous heme IX are published, and a comparison with horseradish peroxidase and cytochrome *c* oxidase [CO photolysis difference spectra, high-spin ferrous heme IX, and heme a_3 (*24*, *25*)] should be

useful. The putative vibrations of the heme propionic acid groups may be seen at 1704/1694 cm^{-1} in H_2O and 1703/1693 cm^{-1} in D_2O (Figure 2). A comparable propionic acid vibration is also seen in nNOS, horseradish peroxidase, and cytochrome *c* oxidase (*25*) photolysis and redox difference spectra (*44*, *45*). The 1 cm^{-1} shift of this feature in the eNOS spectrum on H−D exchange is similar to the equivalent in nNOS and cytochrome *c* oxidase, and has been discussed in detail (*46*). Other heme vibrations at 1405−1407 cm^{-1} [ν(C*a*N)] and 1237−1240 cm^{-1} [δ(C*m*H)] are common to most protein-bound and model heme groups, demonstrating that they are only slightly influenced by their protein environment, as might be expected for internal vibrational modes of the heme macrocycle (*27*, *42*, *43*, *47*). However, in the photolysis difference spectrum of horseradish peroxidase and cytochrome *c* oxidase, the feature at 1405−1407 cm^{-1} is weak or absent (*25*). In nNOS and eNOS, the 1405 cm^{-1} region is dominated by ν_s of carboxylates and ν(CN) of asparagine and glutamine. There are possible heme vibrations in the region of 1237−1240 cm^{-1} [δ(C*m*H), Figure 2 and Table 1]. The latter feature is also present in horseradish peroxidase and nNOS (*24*). Other reported heme vibrational assignments are ν (C*a*C*b*) at 1608 cm^{-1}, ν (C*a*C*m*) at 1548 cm^{-1}, and ν (C*b*C*b*) at 1532 cm^{-1}; the first two are in regions of the spectrum dominated by the amide I and amide II bands, but there are strong discrete vibrations in the region of 1538 cm^{-1} [ν(C*b*C*b*)] in eNOS, nNOS, horseradish peroxidase, and cytochrome *c* oxidase CO photolysis difference spectra (Figure 2; *24*, *25*), which are noted in Table 1.

Substrate Arginine and Its Ligation. Arginine is present in all experiments herein; without it, the enzyme is labile under the reducing conditions that are used. Arginine has vibrations in its guanidinium, carboxylate, and amino groups that may appear in the photolysis difference spectra. The guanidinium ν_{as} of the substrate arginine bound to eNOS probably appears in the photolysis spectra of eNOS, in the vibration at 1691/1684 cm^{-1}; this shifts to 1621/1602 cm^{-1} in D_2O (Figure 2) (*40*, *41*, *48*). Strong differences at 1693/1684 and 1620/1604 cm^{-1} in the H_2O minus D_2O double difference spectrum further support these assignments (Figure 2C). Even stronger evidence for the guanidinium assignments comes from the difference spectra for [$^{14}N/^{15}N$](guanidinium)-arginine photolysis spectra. In Figure 4A, the ν_{as} of the [^{15}N]guanidinium would be expected to contribute to the large 1667/1649 cm^{-1} feature. In the $^{14}N-^{15}N$ double difference spectrum (Figure 4B), the guanidinium ^{14}N ν_{as} and ^{15}N ν_{as} differences maybe seen at 1696/1687 and 1676/1659 cm^{-1}, respectively. The guanidinium ^{14}N ν_s and ^{15}N ν_s may be seen in the double difference spectra at 1647/1636/1625 cm^{-1}; also included in this region (∼1650 cm^{-1}) will be any contribution from the backbone carbonyl which is H-bonded to the guanidinium. The difference in vibration seen at 1400 cm^{-1} in Figure 4B and 1403 cm^{-1} in Figure 5B is probably due to the ν_s of the carboxylate of the glutamate (E363) residue which is H-bonded to the guanidinium (+3 cm^{-1} shift on deutration). The heme(II)−CO ν_{C-O} spectra ($^{14}N-^{15}N$) also give differences (Figures 4B and 5B) that can be attributed to a small shift caused by the $^{14}N-^{15}N$ substitution. The results shown in Figures 4B and 5B indicate the vibrations that can be assigned to the guanidinium group and also suggest that its H-bonding partners, the carboxylate of glutamate (E363), the heme(II)−CO ν_{C-O}, and a backbone carbonyl, are sensitive to the $^{14}N-^{15}N$ substitution.

Asparagine 368. In eNOS, asparagine N368 is H-bonded to the carboxylate of substrate arginine (Figure 7); in nNOS, this position is occupied by an aspartate. A comparison of the photolysis difference spectra of the two isoforms is shown in Figure 6. This carboxamide could contribute to the sharp features at 1408/1397 cm^{-1} (Figure 2A, H_2O) and 1409/1398 cm^{-1} (Figure 2B, D_2O). This assignment is supported by the eNOS−nNOS double difference spectra in Figure 6C (H_2O) (at 1408/1398 cm^{-1}) and Figure 6D (D_2O) (at 1409/1398 cm^{-1}). Underlying these sharp features in the difference spectra is a broader component which may represent the ν_s of the carboxylates. With a clearly different H-bonding network at the substrate binding site in the two isoforms, the double difference spectra will contain more vibrational differences than can be assigned to asparagines and aspartate alone. This illustrates limitations in the applicability of site-directed mutagenesis as an approach to the resolution of FTIR spectra.

In summary, an analysis of the photolysis difference spectrum of eNOS and comparisons of H−D exchange, [$^{14}N/^{15}N$](guanidinium)-arginine with nNOS, allows a range of assignments of vibrations to be suggested with different levels of confidence for elements of the H-bond network around the active site. The [$^{14}N/^{15}N$]guanidinium-arginine substitution is the most useful in assisting identifying vibrations due to the guanidinium group and H-bond partners. Further work using isotopically labeled auxotrophs is needed to strengthen other assignments.

ACKNOWLEDGMENT

We are grateful to Masayo Iwaki for access to unpublished data on the FTIR of model compounds.

REFERENCES

1. Ignarro, L. J., Buga, G. M., Wood, K. S., Byrns, R. E., and Chadhuri, G. (1987) Endothelium derived relaxing factor produced and released from artery and vein is nitric oxide, *Proc. Natl. Acad. Sci. U.S.A. 84*, 9265−9269.
2. Palmer, R. M. J., Ferringe, D. S., and Moncada, S. (1987) Nitric oxide release accounts for the biological activity of endothelial relaxing factor, *Nature 327*, 524−526.
3. Furchgott, R. F., Khan, M. T., and Jothianandan, D. (1987) Comparison of endothelium-dependent relaxation and nitric oxide induced relaxation in rabbit aorta, *FASEB J. 46*, 385−385.
4. Moncada, S., Palmer, R. M., and Higgs, E. A. (1989) Biosynthesis if nitric oxide from L-arginine: A pathway for the regulation of cell function and communication, *Biochem. Pharmacol. 38*, 1709−1715.
5. Ignarro, L. J. (1990) Biosynthesis and metabolism of endothelium derived nitric oxide, *Annu. Rev. Pharmacol. Toxicol. 30*, 535−560.
6. Nathan, C., and Xie, Q. W. (1994) Regulation of biosynthesis of nitric oxide, *J. Biol. Chem. 269*, 13725−13728.
7. MacMicking, J., Xie, Q. W., and Nathan, C. (1997) Nitric oxide and macrophage function, *Annu. Rev. Immunol. 15*, 323−350.
8. Griffith, O. W., and Stuehr, D. J. (1995) Nitric oxide synthases: Properties and catalytic mechanism, *Annu. Rev. Physiol. 57*, 707−736.
9. Hibbs, J. B., Taintor, R. R., and Vavrin, Z. (1987) Macrophage cytotoxicity: Role for L-arginine deiminase and imino nitrogen oxidation to nitrite, *Science 235*, 473−476.
10. Marletta, M. A. (1993) Nitric oxide synthase structure and mechanism, *J. Biol. Chem. 268*, 12231−12234.
11. Stuehr, D. J., Kwon, N. S., Nathan, C. F., Griffith, O. W., Feldman, P. L., and Wiseman, J. (1991) N-ω-Hydroxy-L-arginine is an

intermediate in the biosynthesis of nitric oxide from L-arginine, *J. Biol. Chem. 266*, 6259−6263.
12. Ghosh, D. K., Abu-Soud, H. M., and Stuehr, D. J. (1996) Domains of macrophage N(O) synthase have divergent roles in forming and stabilizing the active dimeric enzyme, *Biochemistry 35*, 1444−1449.
13. Sheta, E. A., McMillan, K., and Masters, B. S. (1994) Evidence for a bidomain structure of constitutive cerebellar nitric oxide synthase, *J. Biol. Chem. 269*, 15147−15153.
14. Ghosh, D. K., and Stuehr, D. J. (1995) Macrophage NO synthase: Characterization of isolated oxygenase and reductase domains reveals a head-to-head subunit interaction, *Biochemistry 34*, 801−807.
15. Bredt, D. S., Hwang, P. M., Glatt, C. E., Lowenstein, C., Reed, R. R., and Snyder, S. H. (1991) Cloned and expressed nitric oxide synthase structurally resembles cytochrome P-450 reductase, *Nature 351*, 714−718.
16. Zhang, J., Martasek, P., Pascjke, R., Shea, T., Siler Masters, B. S., and Kim, J. J. (2001) Crystal structure of the FAD/NADPH-binding domain of rat neuronal nitric oxide synthase. Comparisons with NADPH-cytochrome p450 oxidoreductase, *J. Biol. Chem. 276*, 37506−37513.
17. Crane, B. R., Rosenfeld, R. J., Arvai, A. S., Ghosh, D. K., Ghosh, S., Tainer, J. A., Stuehr, D. J., and Getzoff, E. D. (1999) N-Terminal domain swapping and metal ion binding in nitric oxide synthase dimerization, *EMBO J. 18*, 6271−6281.
18. Li, H., Raman, C. S., Glaser, C. B., Blasko, E., Young, T. A., Parkinson, J. F., Whitlow, M., and Poulos, T. L. (1999) Crystal structures of zinc-free and -bound heme domain of human inducible nitric-oxide synthase: Implications for dimer stability and comparison with endothelial nitric-oxide synthase, *J. Biol. Chem. 274*, 21276−21284.
19. Raman, C. S., Li, H., Martasek, P., Krial, V., Masters, B. S., and Poulos, T. L. (1998) Crystal structure of constitutive endothelial nitric oxide synthase: A paradigm for pterin function involving a novel metal center, *Cell 95*, 939−950.
20. Fischmann, T. O., Hruza, A., Da Niu, X., Fossetta, J. D., Lunn, C. A., Dolphin, E., Prongay, A. J., Reichart, P., Lundell, D., Narula, S. K., and Weber, P. C. (1999) Structural characterization of nitric oxide synthase isoforms reveals striking active-site conservation, *Nat. Struct. Biol. 6*, 233−242.
21. Abu-Soud, H. M., Wang, J., Rousseau, D. L., and Stueher, D. J. (1999) Stopped-flow analysis of substrate binding to neuronal nitric oxide synthase, *Biochemistry 38*, 12446−12451.
22. Couture, M., Stuehr, D. J., and Rousseau, D. L. (2000) The ferrous dioxygen complex of the oxygenase domain of neuronal nitric-oxide synthase, *J. Biol. Chem. 275*, 3201−3205.
23. Couture, M., Adak, S., Stuehr, D. J., and Rousseau, D. L. (2001) Regulation of the properties of the heme-NO complexes in nitric-oxide synthase by hydrogen bonding to the proximal cysteine, *J. Biol. Chem. 276*, 38280−38288.
24. Ingledew, W. J., Smith, S. M. E., Salerno, J. C., and Rich, P. R. (2002) Neuronal nitric oxide synthase ligand and protein vibrations at the substrate binding site. A study by FTIR, *Biochemistry 41*, 8377−8384.
25. Rich, P. R., and Breton, J. (2001) FTIR studies of the CO and cyanide adducts of fully reduced bovine cytochrome *c* oxidase, *Biochemistry 40*, 6441−6449.
26. Alben, J. O., Moh, P. P., Flamingo, F. G., and Altschuld, R. A. (1981) Cytochrome oxidase (a3) heme and copper observed by low-temperature Fourier transform infrared spectroscopy of the CO complex, *Proc. Natl. Acad. Sci. U.S.A. 78*, 234−237.
27. Balasubramanian, S., Lambright, D. G., and Boxer, S. (1993) Perturbations of the distal heme pocket in human myoglobin mutants probed by infrared spectroscopy of bound CO: Correlation with ligand binding kinetics, *Proc. Natl. Acad. Sci. U.S.A. 90*, 4718−4722.
28. Park, S., Pan, L.-P., Chan, S. I., and Alben, J. O. (1996) Photoperturbation of the heme a_3-cuB binuclear center of cytochrome *c* oxidase CO complex observed by Fourier transform infrared spectroscopy, *Biophys. J. 71*, 1036−1047.
29. Hill, J. J., Gennis, R. B., and Alben, J. O. (1992) The heme-copper binuclear center of *Escherichia coli* cytochrome *o* studied by Fourier transform infrared spectroscopy at low temperature, *FASEB J. 6*, A203.
30. Stavrakis, S., Koutsoupakis, K., Pinakoulaki, E., Urbani, A., Saraste, M., and Varotsis, C. (2002) Decay of the transient Cu(B)-CO complex is accompanied by formation of the heme Fe−CO complex of cytochrome *cbb*$_3$-CO at ambient temperature: Evidence from time-resolved Fourier transform infrared spectroscopy, *J. Am. Chem. Soc. 124*, 3814−3815.
31. McMillan, K., Bredt, D. S., Hirsch, D. J., Snyder, S. H., Clark, J. E., and Masters, B. S. (1992) Cloned, expressed rat cerebellar nitric oxide synthase contains stoichiometric amounts of heme, which binds carbon monoxide, *Proc. Natl. Acad. Sci. U.S.A. 89*, 11141−11145.
32. Gross, S. S. (1996) Microtiter plate assay for determining kinetics of nitric oxide synthesis, *Methods Enzymol. 268*, 159−168.
33. Downer, N. W., Bruchman, T. J., and Hazzard, J. H. (1986) Infrared spectroscopic study of photoreceptor membrane and purple membrane. Protein secondary structure and hydrogen deuterium exchange, *J. Biol. Chem. 261*, 3640−3647.
34. Glasoe, P. K., and Long, F. A. (1960) Use of glass electrodes to measure acidities in deuterium oxide, *J. Phys. Chem. 64*, 188−190.
35. Rath, P., DeGrip, W. J., and Rothschild, J. (1998) Photoactivation of Rhodopsin Causes an Increased Hydrogen−Deuterium Exchange of Buried Peptide Groups, *Biophys. J. 74*, 192−198.
36. Jung, C., Stuehr, D. J., and Ghosh, D. K. (2000) FT-infrared spectroscopic studies of the iron ligand CO stretch mode of iNOS oxygenase domain: Effect of arginine and tetrahydrobiopterin, *Biochemistry 39*, 10163−10171.
37. Scheele, J. S., Kharitonov, V. G., Martasek, P., Roman, L. J., Sharma, V. S., Masters, B.-S., and Magde, D. (1997) Kinetics of CO ligation with nitric-oxide synthase by flash photolysis and stopped-flow spectrophotometry, *J. Biol. Chem. 272*, 12523−12528.
38. Abu-Soud, H. M., Wu, C., Ghosh, D. K., and Stuehr, D. J. (1998) Stopped-flow analysis of CO and NO binding to inducible nitric oxide synthase, *Biochemistry 37*, 3777−3786.
39. Smith, S. M. E., Sham, C., Roman, L., Martasek, P., and Salerno, J. C. (2001) Titration of low Kd binding sites: Binding of arginine analogs to nitric oxide synthases, *Nitric Oxide J. 5* (5), 442−452.
40. Barth, A. (2000) The infrared absorption of amino acid side chains, *Prog. Biophys. Mol. Biol. 74*, 141−173.
41. Venyaminov, S. Y., and Kalnin, N. N. (1990) Quantitative IR spectrophotometry of peptide compounds in water (H_2O) solutions. I. Spectral parameters of amino acid residue absorption bands, *Biopolymers 30*, 1243−1257.
42. Alben, J. O. (1978) Infrared spectroscopy of porphyrins, in *The Porphyrins* (Dolphin, D., Ed.) Vol. III, pp 323−346, Academic Press, New York.
43. Felton, R. H., and Yu, N.-T. (1978) Resonance Raman scattering from metalloporphtrins and hemoproteins, in *The Porphyrins* (Dolphin, D., Ed.) Vol. III, pp 347−388, Academic Press, New York.
44. Berthomieu, B., Boussac, A., Mantele, W., Breton, J., and Naberdryk, E. (1992) Molecular changes following oxidoreduction of cytochrome *b559* characterized by Fourier transform infrared difference spectroscopy and electron paramagnetic resonance: Photooxidation in photosystem II and electrochemistry of isolated cytochrome b559 and iron protoporphyrin IX-bisimidazole model compounds, *Biochemistry 31*, 11460−11471.
45. Puustinen, A., Bailey, J. A., Dyer, R. B., Mecklenburg, S. L., Wikstrom, M., and Woodruff, W. H. (1997) Fourier Transform Infrared Evidence for Connectivity Between CuB and Glutamic-Acid-286 in Cytochrome *bo*$_3$ from *Escherichia coli*, *Biochemistry 36*, 13195−13200.
46. Okuno, D., Iwase, T., Shinzawa-Itoh, K., Yoshikawa, S., and Kitagawa, T. (2003) FTIR detection of protonation/deprotonation of key carboxyl side chains caused by redox change of the Cu(A)-heme a moiety and ligand dissociation from the heme a_3−Cu(B) center of bovine heart cytochrome *c* oxidase, *J. Am. Chem. Soc. 125*, 7209−7218.
47. Iwaki, M., Giotta, L., Akinsiku, A. O., Schagger, H., Fisher, N., Breton, J., and Rich, P. R. (2003) Redox-induced transitions in bovine cytochrome *bc*$_1$ complex studied by perfusion-induced ATR-FTIR spectroscopy, *Biochemistry 42*, 11109−11119.
48. Rudiger, M., Haupts, U., Gerwert, K., and Oesterhelt, P. (1995) Chemical reconstitution of a chloride pump inactivated by a single point mutation, *EMBO J. 14*, 1599−1606.

BI047891Y